Applied Organometallic Chemistry

WILEY

Applied Organometallic Chemistry

RESEARCH ARTICLE OPEN ACCESS

Design and Synthesis of a Novel Catalytic System Based on Pd Supported on Alumina Extrudates for Hydrotreating of PAO Lubricants

Mahsa Karimi[1] | Samahe Sadjadi[1] | Hassan Arabi[1] | Naeimeh Bahri-Laleh[1,2,3] | Albert Poater[4]

[1]Iran Polymer and Petrochemical Institute, Tehran, Iran | [2]RIKEN Center for Emergent Matter Science (CEMS), Saitama, Japan | [3]Institute for Sustainability with Knotted Chiral Meta Matter (WPI-SKCM[2]), Hiroshima University, Hiroshima, Japan | [4]Institut de Química Computacional i Catàlisi and Departament de Química, Universitat de Girona, Girona, Catalonia, Spain

Correspondence: Samahe Sadjadi (s.sadjadi@ippi.ac.ir) | Naeimeh Bahri-Laleh (nbahri@hiroshima-u.ac.jp)

Received: 24 May 2024 | **Revised:** 5 August 2024 | **Accepted:** 16 August 2024

Funding: A.P. is a Serra Húnter Fellow and was supported by the Institució Catalana de Recerca i Estudis Avançats (ICREA) Academia Prize 2019 and thanks the Spanish Ministerio de Ciencia, Innovación y Universidades (MINECO) for project PID2021-127423NB-I00 and the Generalitat de Catalunya for project 2021SGR623. Computational time at the MARENOSTRUM supercomputer (QHS-2022-3-0029) has been provided by the Barcelona Supercomputing Centre through a grant from Red Española de Supercomputación.

Keywords: catalyst | extruded support | hydrogenation reaction | polyalphaolefin | γ- alumina

ABSTRACT

The development of hydrogenation processes for polyalphaolefin (PAO) lubricants, which hold commercialization potential, is a challenging endeavor. Here, we synthesized and characterized rod-shaped γ-alumina supported Pd catalyst for PAO hydrofinishing, comparing it with γ-alumina supported Ni catalyst. Results indicated that Pd/Al_2O_3 catalyst efficiently promoted PAO hydrofinishing, whereas Ni-based catalyst exhibited lower activity. Optimization of reaction variables using the one-factor-at-a-time method revealed that hydrogenated polyalphaolefin could be achieved with a 90% yield using a 5 wt.% catalyst, a hydrogen pressure of 12 bar, at 130°C after 7 h. The superior performance of the fabricated catalysts, coupled with the use of rod-shaped alumina suitable for large-scale hydrogenation reactors, suggests the versatility of the process for potential commercialization. Additionally, the higher performance of Pd/alumina compared to Ni/alumina catalyst was computationally assessed at the molecular level using DFT methods.

1 | Introduction

Base oils are obtained by refining crude oils. A large number of crude oils are used around the world to produce base oils. In this field, fluids based on polyalphaolefins (PAOs) have received great attention in recent years due to their outstanding properties. Compared to mineral oils, PAOs benefit from low pour points, high viscosity index (VI), low toxicity, compatibility with mineral oils, better oxidation stability, low corrosion, high shear, and thermal and hydrolytic stability [1–5]. In general, a three-stage process is necessary to obtain final PAOs, including oligomerization, hydrogenation, and distillation to achieve different grades. Crude PAOs from oligomerization contain olefinic bonds in their backbone (−C=C) that are prone to oxidation at high temperatures. Therefore, the hydrogenation process is highly important to complete the saturation of the oligomeric chains. On the other hand, crude PAO hydrofinishing usually needs harsh conditions (> 30 bar, > 200°C) under precious metals catalysis. This issue enhances the risk and cost of PAO production. Like other hydrogenation processes, there are two essential factors for the hydrogenation of PAO base oils, hydrogen source, and a catalyst. Due to the importance of economic issues in large-scale processes, choice of an efficient catalytic system is imperative to operate under

mild reaction conditions with low precious metals loading in the hydrofinishing reaction and use of low hydrogen pressure [6, 7]. Palladium-catalyzed reactions have received increasing attention in the last decades [8–11]. Because of more facile recovery and superior recyclability, the heterogeneous catalysts have attracted great attention in many industrial operations. In these catalysts, the type of support and support synthesis could affect the catalyst performance [12]. Different kinds of materials, such as clays, silica, and polymers, could be used as catalytic supports [13, 14]. One of the extensively utilized catalytic supports in chemical reactions is alumina (Al_2O_3), which benefits from appealing features, such as high mechanical resistance, reasonable stability, and low cost. Among different types of aluminas, γ-alumina is a fascinating material, which has found extensive use as a commercial catalyst and catalyst support in the chemical and petrochemical industries [15, 16]. This may probably be related to its improved properties, such as high thermal stability, moderate wear resistance, specific surface area, pore size, and pore volume. In order to control the stability and textural features of a catalyst, the wise choice of support and its shaping are essential [17]. Catalyst based on extruded supports [18, 19], instead of the powder forms, could be an excellent choice for many industrial applications. These catalysts with different geometrical forms are charming due to ease of transport, good mechanical properties, and easier recyclability [20–22].

In the pursuit of our study on PAO hydrogenation catalysts [23, 24], herein we wish to report the synthesis of a heterogeneous Pd-based catalyst using extruded γ-alumina support, Pd/γ-Al_2O_3 catalyst. The catalytic performance of Pd/γ-Al_2O_3 catalyst in hydrotreating of PAO was studied and compared with that of Ni/γ-Al_2O_3 catalyst, and the reaction variables were optimized to achieve the highest yield of hydrogenated PAO (H-PAO). Density functional theory (DFT) calculations provide a mechanistic understanding of why Pd exhibits significantly superior performance compared to Ni. This insight could guide future experimental studies [25, 26], leveraging predictive catalysis approaches before conducting the calculations.

2 | Experimental

γ-Alumina, boehmite, and polyethylene glycol 400 (PEG 400) were supplied from Merck Co., Germany. Nitric acid (HNO_3), $Pd(OAc)_2$, $NiN_2O_6.6H_2O$, $NaBH_4$, methanol, and toluene were purchased from Sigma-Aldrich and used with no further purification. To synthesize PAO, the following reagents were utilized: $AlCl_3$, 1-decene (94%), and NaOH, provided by Merck Co., Germany.

2.1 | Characterization

To ensure the formation of the desired catalyst, the following characteristic techniques were used: ICP-AES, wide-angle x-ray scattering (WAXS), Fourier transform infrared (FTIR), Brunauer–Emmett–Teller (BET), TGA, SEM, energy-dispersive spectroscop (EDS), and elemental mapping analyses. More precisely, to measure the Pd loading of the catalyst, ICP-AES (Varian, Vista Pro) was carried out.

The FTIR spectrum of the catalyst was scanned by PerkinElmer Spectrum 65 using the KBr pellet technique. WAXS was accomplished on a D5000 Siemens apparatus using Cu-Kα radiation to survey the structural properties of the catalyst. The catalyst

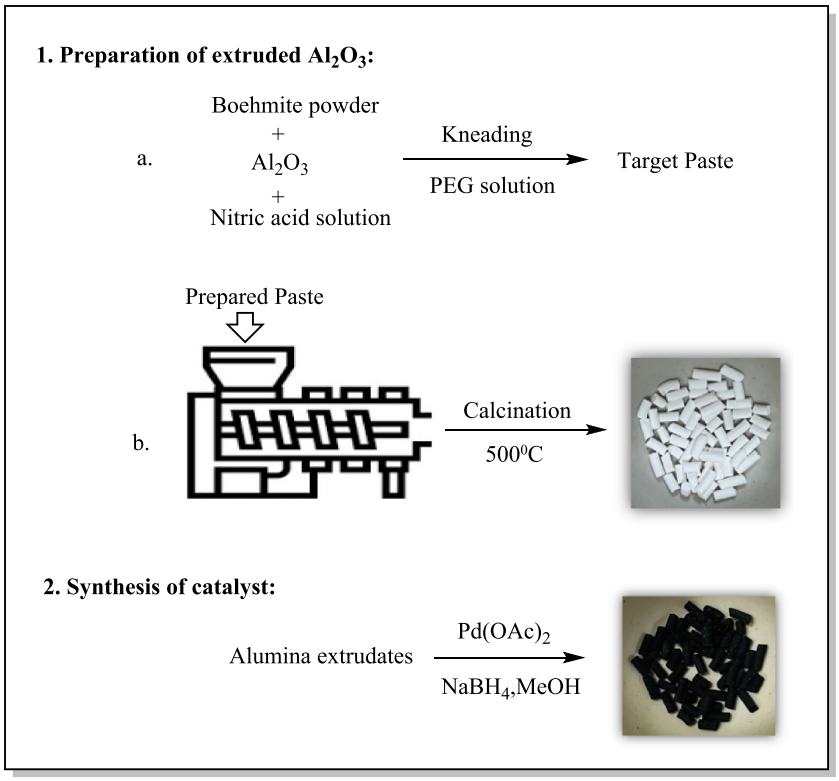

FIGURE 1 | Scheme of the catalytic synthetic procedure.

was examined at room temperature between 10° and 80° with 0.02° intervals. To investigate the thermal properties of the catalyst, its thermogravimetric (TG) curve was recorded via Mettler Toledo apparatus. For this purpose, the catalyst was heated from room temperature to 800°C with a heating rate of 10°C·min^{-1} under O_2 atmosphere. BET was applied to study the surface properties of the catalyst. A Santam STM-20 machine was used to determine the crushing strength of the catalyst. The morphology of the catalyst was investigated using the VEGAII TESCAN scanning electron microscope (SEM). EDS and mapping analyses were also performed. Molecular weights and polydispersity index (PDI) of the synthesized oil were determined by gel permeation chromatography (GPC Agilent 1100). Viscosity index (VI) and kinematic viscosities at 40°C and 100°C (KV40 and KV100) were also obtained using ASTM D 97 and ASTM D445, respectively. To estimate the degree of hydrogenation yield, ^{1}HNMR spectroscopy was performed using Bruker DRX400MHz NMR spectrometer in deuterated chloroform at 25°C.

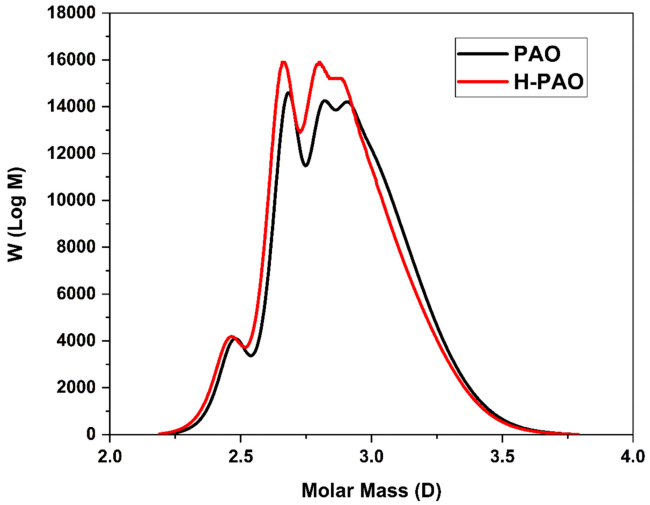

FIGURE 2 | GPC chromatograms of synthesized PAO and H-PAO.

2.2 | Catalyst Preparation

2.2.1 | Synthesis of Support

Alumina extrudates were synthesized according to the previous known procedures [27–29]. In a typical synthesis, the target support was prepared by reacting boehmite powder (3.04 g) with γ-alumina (0.16 g), followed by the addition of nitric acid solution (3 wt.%), as a peptizing agent, and the aqueous solution of PEG 400 (15 wt.%) at room temperature. The mixture was then kneaded to obtain a homogeneous paste. After extortion of the prepared paste, the extruded products were dried at ambient temperature and then at 110°C for 12 h. The formed samples were also calcined in air for 5 h at 500°C (Figure 1). The mechanical strength of this material was studied, and the crushing strength of the as-prepared support was determined as ~422 N.cm^{-2}. According to the surface properties of the synthesized extruded γ-alumina, the values of the specific surface area, average pore diameter, and pore volume were 240.3 m^2.g^{-1}, 8.45 nm, and 0.512 cm^3.g^{-1}, respectively.

2.2.2 | Synthesis of Catalyst

In this step, immobilization of Pd nanoparticles on the extruded Al_2O_3 support was carried out by utilizing the incipient wet impregnation technique [24, 30, 31]. All experiments were carried out at room temperature. After the introduction of toluene into the extruded Al_2O_3, a solution of Pd $(OAc)_2$ (0.03 g) in toluene (15 mL) was added dropwise, and the resulting mixture was gently stirred overnight. In order to reduce Pd(II) to Pd(0), a solution of $NaBH_4$ (0.11 g) in methanol (15 mL) was slowly added under stirring to the aforesaid mixture. The solution was allowed to mix slowly overnight. The solvent was then removed to afford the catalyst (Figure 1). The loading of Pd was 1.3 wt.%, which was confirmed by ICP analysis. It is worth mentioning that the extruded Al_2O_3 did not

TABLE 1 | Hydrotreating of PAO using Pd/γ-Al_2O_3 catalyst.[a]

Run	Catalyst (w/w. %)	Pressure (bar)	Temperature (°C)	Time (h)	Yield (%)
1	2	8	100	5	48
2	3	8	100	5	55
3	5	8	100	5	65
4	6	8	100	5	65
5	5	5	100	5	59
6	5	10	100	5	73
7	5	12	100	5	81
8	5	15	100	5	81
9	5	12	130	5	86
10	5	12	150	5	84
11	5	12	130	7	90
12	5	12	130	9	90

[a]PAO = 10 g.

demonstrate any deformation in the palladation process. As expected, the surface properties of the catalyst, the specific surface area (220 $m^2.g^{-1}$), and the pore volume (0.42 $cm^3.g^{-1}$) declined after the introduction of Pd nanoparticles, which confirmed the infiltration of metallic species into the pores.

Similarly, the Ni/γ-Al_2O_3 catalyst was also synthesized by the same procedure, except with $NiN_2O_6.6H_2O$ (deionized water solution), instead of Pd $(OAc)_2$ as a metal center during the catalyst preparation.

2.3 | Synthesis of PAO

2.3.1 | Oligomerization

The PAO-based lubricant was synthesized according to known procedures reported [32–34]. All experiments were performed under dry nitrogen atmosphere in a 250 mL stainless steel mechanically stirred (1000 rpm) pressure reactor coupled to an oil bath to adjust the temperature. Prior to the oligomerization experiments, the reactor was connected to a high pressure line and degassed. The pressure vessel was heated to 90°C using the oil bath for 1 h. The reactor was charged with the $AlCl_3$ catalyst (5 g), and then monomer solution (500 mL 1-decene in 0.3 mL deionized water) was injected into the oligomerization system via a syringe. After that, the reaction mixture was continued at 100°C for 1 h. Eventually, the volatiles were removed, and the residue was washed with NaOH solution (5 wt.%) several times. According to the GPC chromatogram (Figure 2), the characteristics of the synthesized PAO were as follows: $M_n = 672\ g.mol^{-1}$, $Đ = 1.34$. $KV^{40} = 23.0$, $KV^{100} = 4.8$, and VI = 129.

2.3.2 | Hydrofinishing Process

Like the oligomerization step, the desired reactor was purged under dry nitrogen. Catalyst (5 wt.%) as well as synthetic oil was introduced to the reactor, and the reactor was sealed. Afterwards, hydrogen gas was injected, and the hydrogenation reaction was performed with continuous stirring for 7 h. The hydrogenation experiments with variable reaction conditions can be shown in Table 1. At the end, the reactor was discharged, and the catalyst was filtered. The yield of the hydrogenation was evaluated via ^{1}HNMR spectroscopy of hydrogenated PAO oil.

2.4 | Computational Details

The Gaussian 16 package was used to perform all the DFT calculations [35]. Geometry optimizations were carried out using the pure GGA functional of Becke and Perdew, known as BP86 [36, 37], with explicit dispersion corrections applied through the

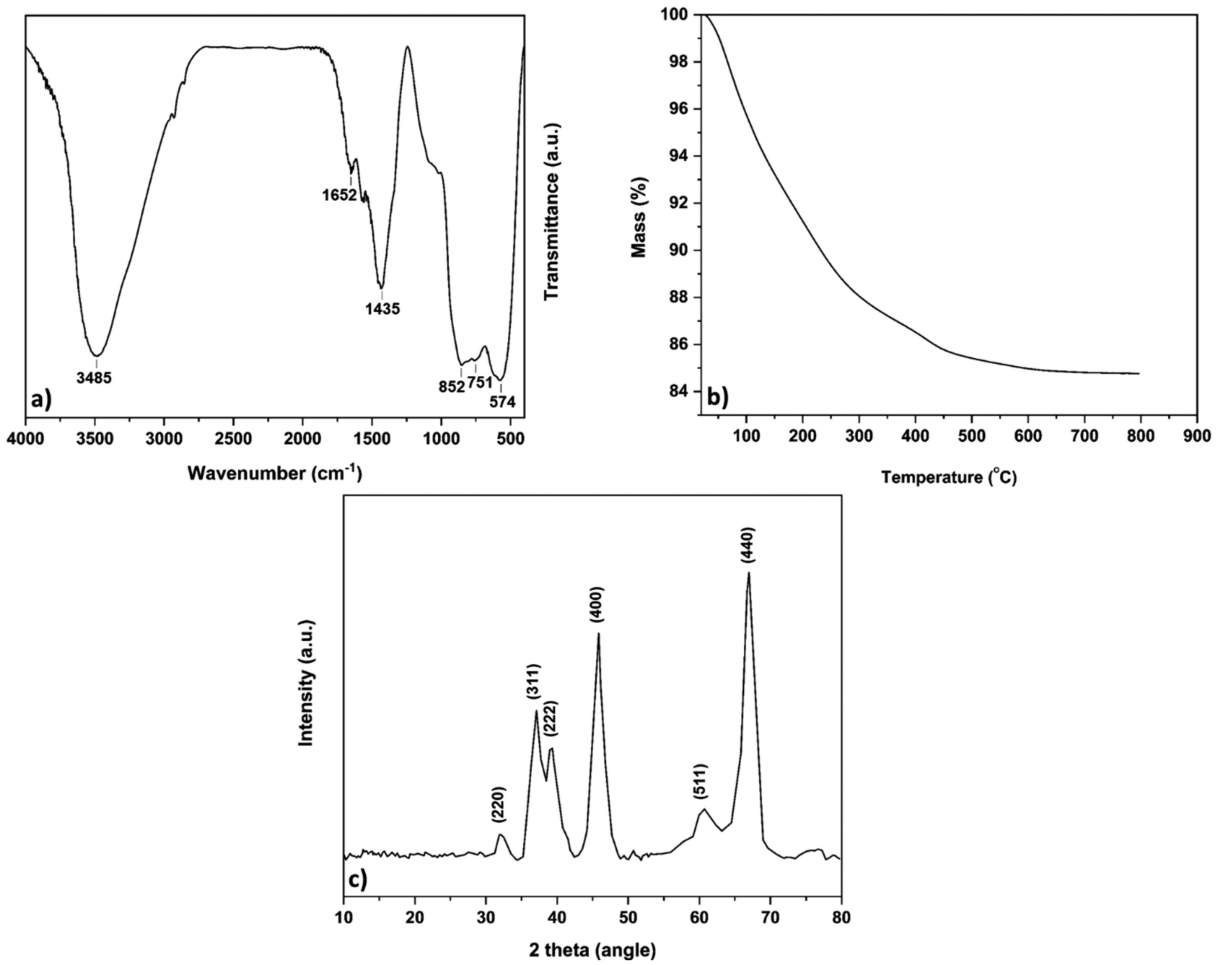

FIGURE 3 | (a) FTIR spectrum, (b) thermogravimetric analysis, and (c) XRD pattern of Pd/γ-Al_2O_3 catalyst.

Grimme D3 method [38]. For non-metal atoms (i.e., C, H, N, O, Al, and Si), the split-valence basis set (Def2SVP keyword in Gaussian) [39, 40] was employed. For Pd, the small-core quasi-relativistic Stuttgart/Dresden effective core potential, with an associated valence basis set (standard SDD keyword in Gaussian16), was used to address relativistic effects [41–43]. Geometry optimizations were performed without symmetry constraints. Additionally, the γ-alumina fragment was optimized as it is known to be non-rigid. A single Pd atom was used to simulate the Pd content on the support system. Analytical frequency calculations were conducted to confirm the nature of the stationary points, whether minima or transition states. Any overestimation of the entropy was investigated using the model by Martin et al. [44] and the implementation by Poater et al. [45–47], applying a pressure of 1354 atm. Furthermore, single-point energy calculations using the hybrid GGA functional of Becke–Lee, Parr, and Yang, specifically B3LYP [48–50] and the cc-pVTZ basis set for the non-metal atoms were performed [51]. The reported Gibbs energies in this work include values obtained at the B3LYP-D3/cc-pVTZ+SDD//BP86-D3/Def2SVP + SDD level of theory, corrected for zero-point energies, thermal corrections, and entropy effects evaluated with the BP86-D3/Def2SVP + SDD method.

3 | Results and Discussion

The as-prepared Pd/γ-Al_2O_3 catalyst was characterized via various characterization techniques. In the following section, the results will be discussed in detail.

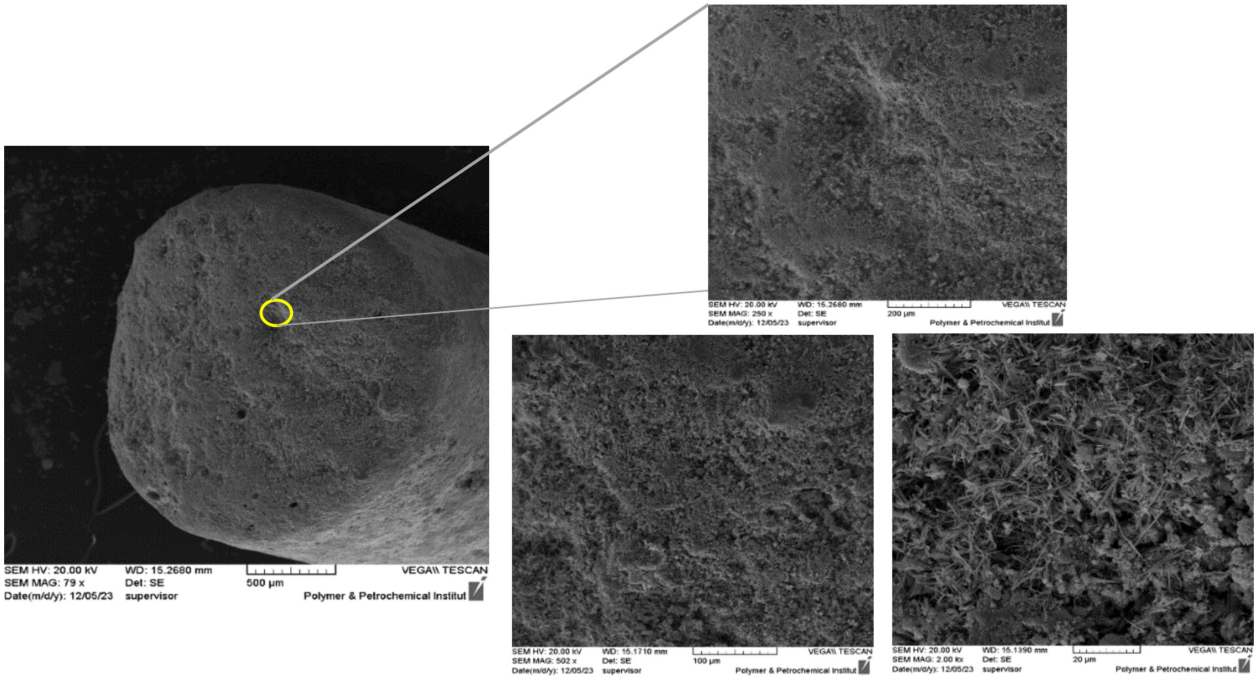

FIGURE 4 | SEM micrographs of the catalyst at different magnifications.

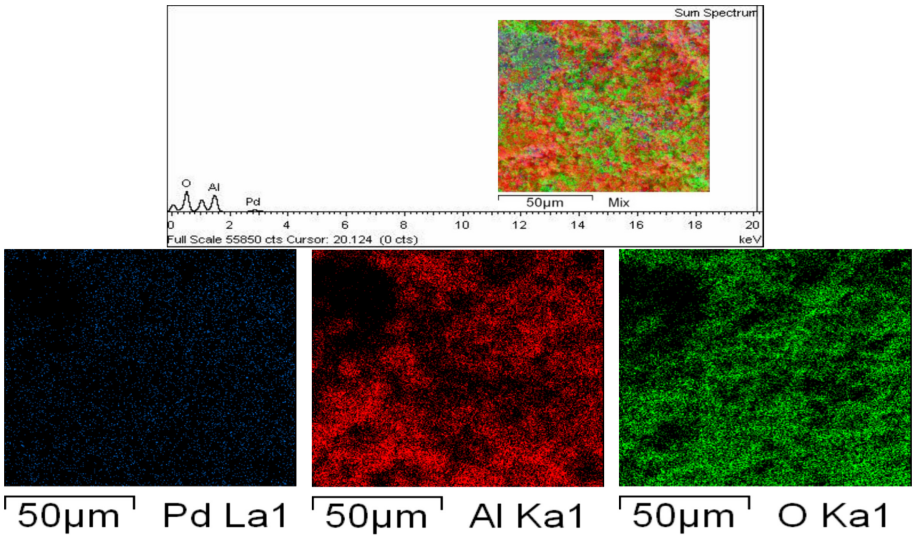

FIGURE 5 | EDS and elemental mapping analyses of catalyst.

3.1 | FTIR Spectrum

To survey the structure of the Pd/γ-Al_2O_3 catalyst, an FTIR analysis was performed. According to Figure 3a, the bands, which appear at 852, 751, and 574 cm^{-1}, are indicative of the Al-O vibration of the γ-form of alumina. The absorption bands at 1652 and 1435 cm^{-1} can be attributed to the stretching and bending vibrations of Al-O, respectively. The broad band at 3400 cm^{-1} is attributed to the Al–OH stretching vibration due to the hydroscopic generation of alumina and hydrogen bonding with water molecules. These observations are in good agreement with the literature and support the formation of γ-Al_2O_3 [52–55]. Notably, the stabilization of Pd nanoparticles on γ-Al_2O_3 cannot be confirmed by FTIR spectroscopy, as the characteristic bands of Pd nanoparticles overlap with those of γ-Al_2O_3.

3.2 | Thermogravimetric Analysis

According to the TG thermogram (Figure 3b), the weight loss at 100°C is attributed to the loss of adsorbed water on the alumina surface. The weight loss between 300°C and 500°C could be associated with the breaking of Al–OH bonds, which confirmed the loss of structural stability and dehydration at elevated temperatures [56, 57]. These results confirm a high thermal stability of the Pd/γ-Al_2O_3 catalyst.

3.3 | XRD Pattern

The XRD pattern of Pd/Al_2O_3 is depicted in Figure 3c. According to the previous studies, the observed peaks in the XRD pattern confirmed the γ-alumina structure [52, 56, 58]. As expected, characteristic peaks at 2θ of 32.10°, 37.10°, 39.43°, 45.90°, 60.72°, and 66.98° are detected, which ae assigned to the (220), (311), (222), (400), (511), and (440) planes of the orthorhombic crystal cell, respectively. Remarkably, the characteristic peaks of Pd nanoparticles were not observed in the XRD pattern of Pd/Al_2O_3, which is due to the low amount of Pd nanoparticles.

3.4 | SEM-EDS

The SEM images of the catalyst are illustrated in Figure 4. As shown, the catalyst exhibited an aggregated-like morphology.

TABLE 2 | Methyl type of the synthesized PAO and H-PAO.

CH_3 type	Chemical shift (ppm)	PAO	H-PAO
CCH_2CH_3	10.9	1	1
$(CH_3)CHCH_2CH_3$	11.3	1	1
$CHCH_2CH_2CH_3$	14.5	4	3
$CH(CH_3)CH_2CH_2CH_3$	14.4	2	2
$(CH_2)nCH_2CH_2CH_3$ $n>1$	14.1	41	41
$CH_2CH(CH_3)CH$	15–17	6	6
$CH_2CH(CH_3)CH_2$	19.7	7	7
$CH_3CH(CH_3)CH_2$	22.7	39	37

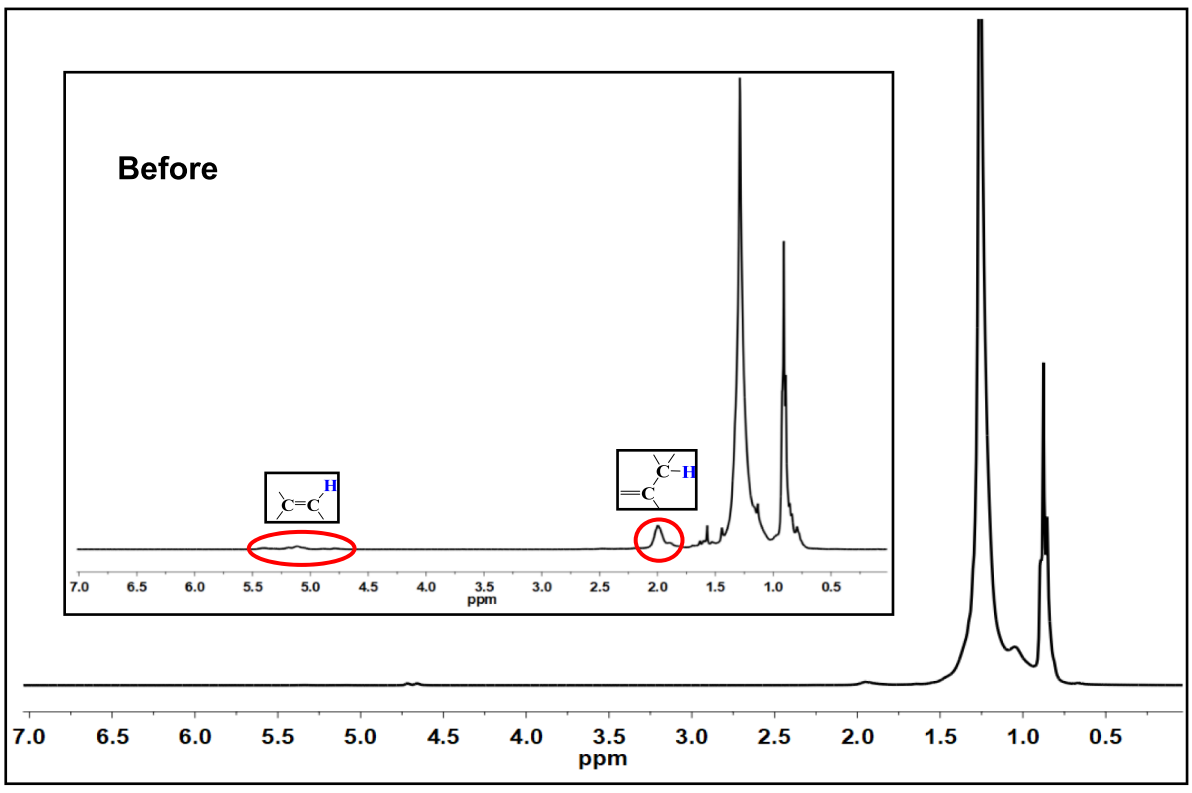

FIGURE 6 | ^{1}HNMR spectra of PAO before and after hydrogenation.

To appraise the surface composition of the catalyst and the dispersion of Pd nanoparticles on γ-Al_2O_3 support, EDS and elemental mapping analyses have also been performed. The existence of Al, O, and Pd atoms in the catalyst structure approves a successful impregnation of Pd species on the support (Figure 5). Moreover, the high dispersion of Pd atoms indicates a uniform palladation of γ-Al_2O_3.

3.5 | Hydrofinishing of PAO

3.5.1 | Effect of Catalytic Species

To determine which catalyst has supperior performance, the activity of the two as-prepared catalysts was studied. In all experiments, the hydrogenation conditions were kept constant, and the degree of hydrofinishing was investigated using ^{1}HNMR. According to the results, the palladium-based catalyst revealed higher performance compared to nickel catalyst in PAO hydrogenation under identical condition (PAO = 10 g, loading catalyst = 5 wt.% of PAO, temp = 130°C, time = 7 h, and H_2 pressure = 12 bar). More precisely, hydrogenation yield of 90% was obtained in the presence of Pd/γ-Al_2O_3, whereas the nickel system, Ni/γ-Al_2O_3, showed the lowest catalytic activity and provided a moderate degree of hydrogenation (58%).

3.5.2 | Optimization of Reaction Variables

As mentioned above, hydrofinishing of PAO oils is highly important in many industrial processes. To optimize the reaction variables of hydrofinishing, the reaction was conducted under the different reaction conditions, and the reaction variables including catalyst loading, hydrogen pressure, temperature and reaction time were optimized. These factors were separately investigated to shed light on their performance in the hydrogenation process, and the results were illustrated in Table 1. To optimize the catalyst loading, the hydrogenation of PAO was accomplished in the different amounts of catalyst (2–6 wt.%) under H_2 pressure of 8 bar at 100°C for 5 h. The reaction yield increased with catalyst dosage up to 5 wt.% and revealed a decline to higher levels. Hence, 5 wt.% of Pd/γ-Al_2O_3 was considered enhancing the efficiency up to 65%.

The effect of the hydrogen pressure on the reaction efficiency was also studied for 5 wt.% of Pd/γ-Al_2O_3 at 100°C for 5 h. More precisely, the hydrogenation yield at the different pressures followed the order of 15, 12 bar (81%) > 10 bar (73%) > 8 bar (65%) > 5 bar (59%). Therefore, the ideal value for this parameter was 12 bar.

In order to further investigate effectiveness of the process, the hydrofinishing was also conducted using 5 wt.% Pd/γ-Al_2O_3 and hydrogen pressure of 12 bar in various temperatures and times. As tabulated, increasing the reaction temperature to 130°C led to an increase in the hydrogenation yield up to 86%. However, the further increase in temperature was not impressive. Similarly, the highest efficiency (90%) was observed when the hydrogenation was prolonged for 7 h rather than 5 h. On the other hand, further increase of this parameter did not have any appreciable change.

As a final result of the optimization experiments, the highest degree of hydrogenation (90%) was obtained in the presence of 5 wt.% of catalyst at 130°C and 12 bar hydrogen pressure for 7 h (Run 11). As observed, these results are in good agreement with the ^{1}HNMR spectrum of the hydrogenated PAO oil shown in Figure 6.

3.5.3 | Characterization of PAO and H-PAO

At the end of this work, to investigate the microstructure of PAO before and after hydrogenation, its molecular weight and type of branching were evaluated. As seen in Figure 2, no significant change in the molecular weight and PDI was observed after the hydrotreating process, $M_n = 665\ g.mol^{-1}$, $Đ = 1.33$. On the other hand, the branching type of the as-synthesized H-PAO was also investigated using ^{13}CNMR spectroscopy and gathered in Table 2. By investigation of the structural analysis, the methyl type did not change considerably after hydrofinishing reaction, which confirmed the absence of any

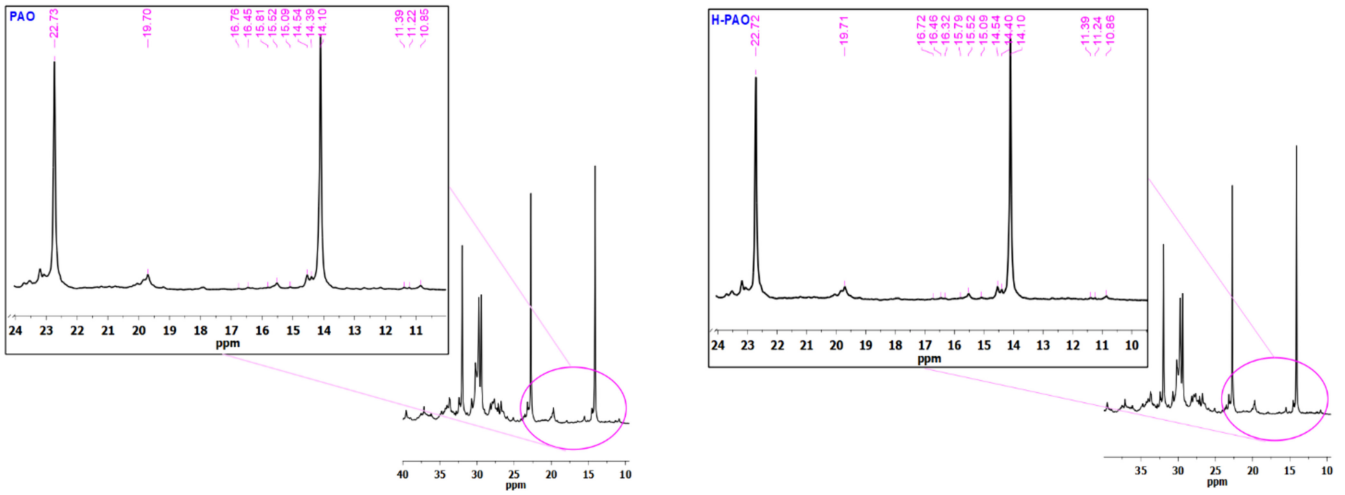

FIGURE 7 | ^{13}CNMR spectra of left:PAO and right:H-PAO.

isomerization. Concluding this part, the results corroborated the high performance of designed catalyst in PAO hydrofinishing (Figure 7).

3.6 | DFT Results

To shed light on why the system with nickel shows minimal or no activity, a study was conducted using DFT. The hydrogenation mechanism with molecular hydrogen was examined in Figure 8, with the metal center that bears three oxygen atoms of the support in a facial way, starting with the simple olefin ethylene. Beginning with the neutral species **I**, either with Pd(0) or Ni(0), the olefin is first incorporated, forming intermediate **II**, with clear thermodynamic stabilization reaching up to 26.2 and 15.9 kcal/mol for Pd and Ni, respectively. Next, molecular hydrogen coordinates with an energy cost exceeding 10 kcal/mol to form intermediate **III**. This intermediate is likely partially fictitious, as the adduct where the diatomic molecule is not coordinated to the metal but exists as a coordination intermediate has energy nearly isoenergetic to the preceding intermediate **II**.

Although the order of olefin and molecular hydrogen coordination can vary, this does not improve the process, as it leads to an alternative intermediate **II** that is even less stable than intermediate **III**. Both strategies ultimately guide to this intermediate **III**. From here, via transition state **III–IV**, one of the hydrogen atoms from the former molecular hydrogen migrates to the nearest methylene group, with an energy barrier of 21.7 and 28.9 kcal/mol for Pd and Ni, respectively. This already indicates a preference for Pd. Using Kozuch and collaborators' rate-determining state (rds) criterion, which considers the energy of the rate determining intermediate (rdi), instead of the relatively unstable intermediate **III**, the energy barriers are 35.9 and 49.1 kcal/mol for Pd and Ni, respectively, further highlighting the higher kinetic cost for Ni. And to close the catalytic cycle, following the hydrogen migration in intermediate **IV**, the

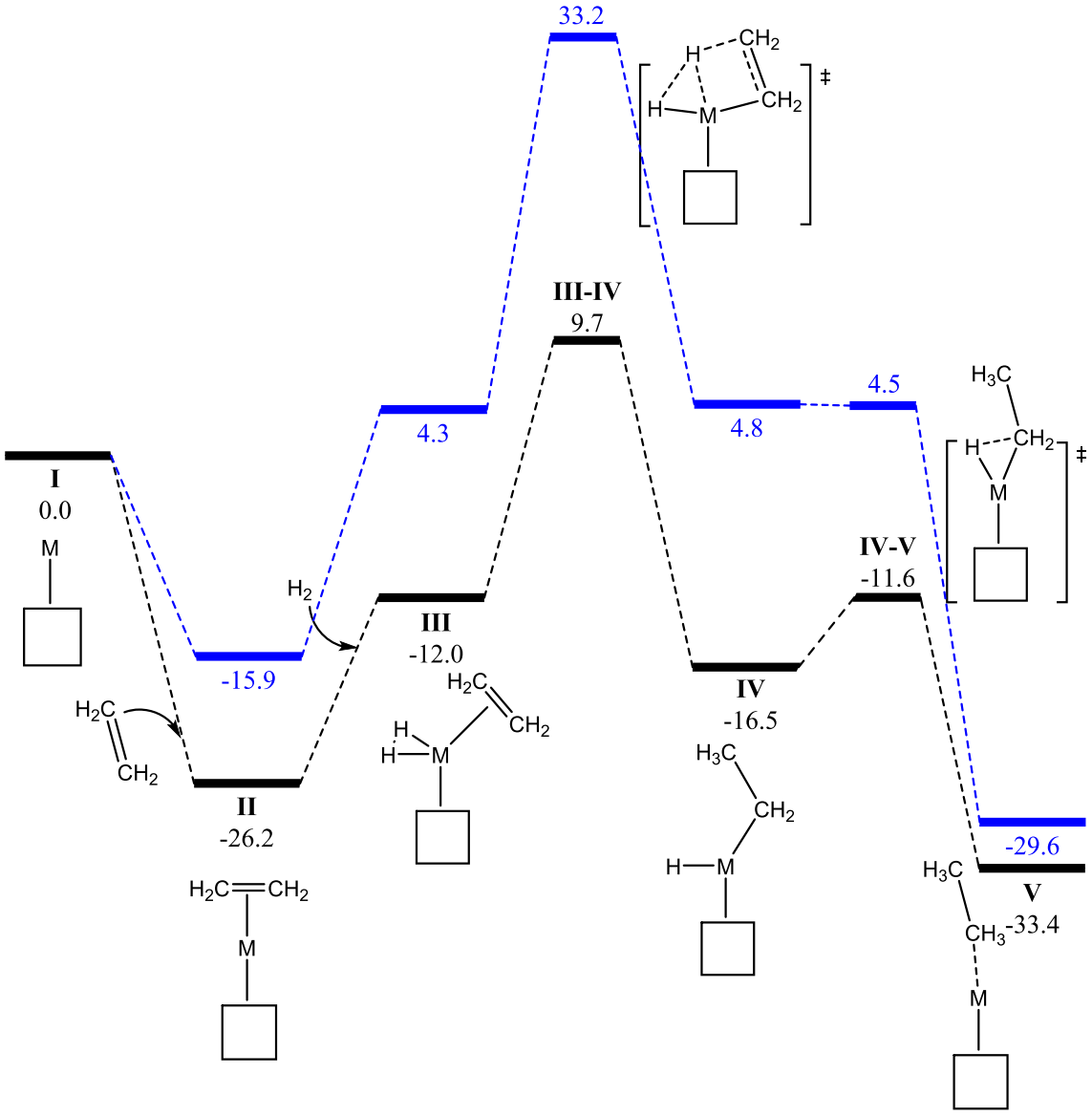

FIGURE 8 | Reaction pathway for the hydrogenation of ethylene, showing relative Gibbs energies in kcal/mol (the cube represents the truncated γ-alumina, energies in black and blue for Pd and Ni, respectively).

second hydrogen must also migrate to form the ethane molecule, transferring the remaining hydride in intermediate **IV** to the alkyl moiety CH_2CH_3. This transition state **IV–V** requires 4.9 kcal/mol for Pd and is barrierless for Ni. Interestingly, it thermodynamically leads to an over-stabilized adduct of the M(0) species, with stabilization of 33.4 and 29.6 kcal/mol for Pd and Ni, respectively. This aligns perfectly with the exergonic transformation of ethylene and hydrogen to ethane, releasing up to 28.9 kcal/mol. On the other hand, because the ^{13}CNMR spectra did not reveal chain walking [59, 60], we excluded this alternative reaction with Pd, knowing that the hydrogenation barriers should be higher to promote to it [61].

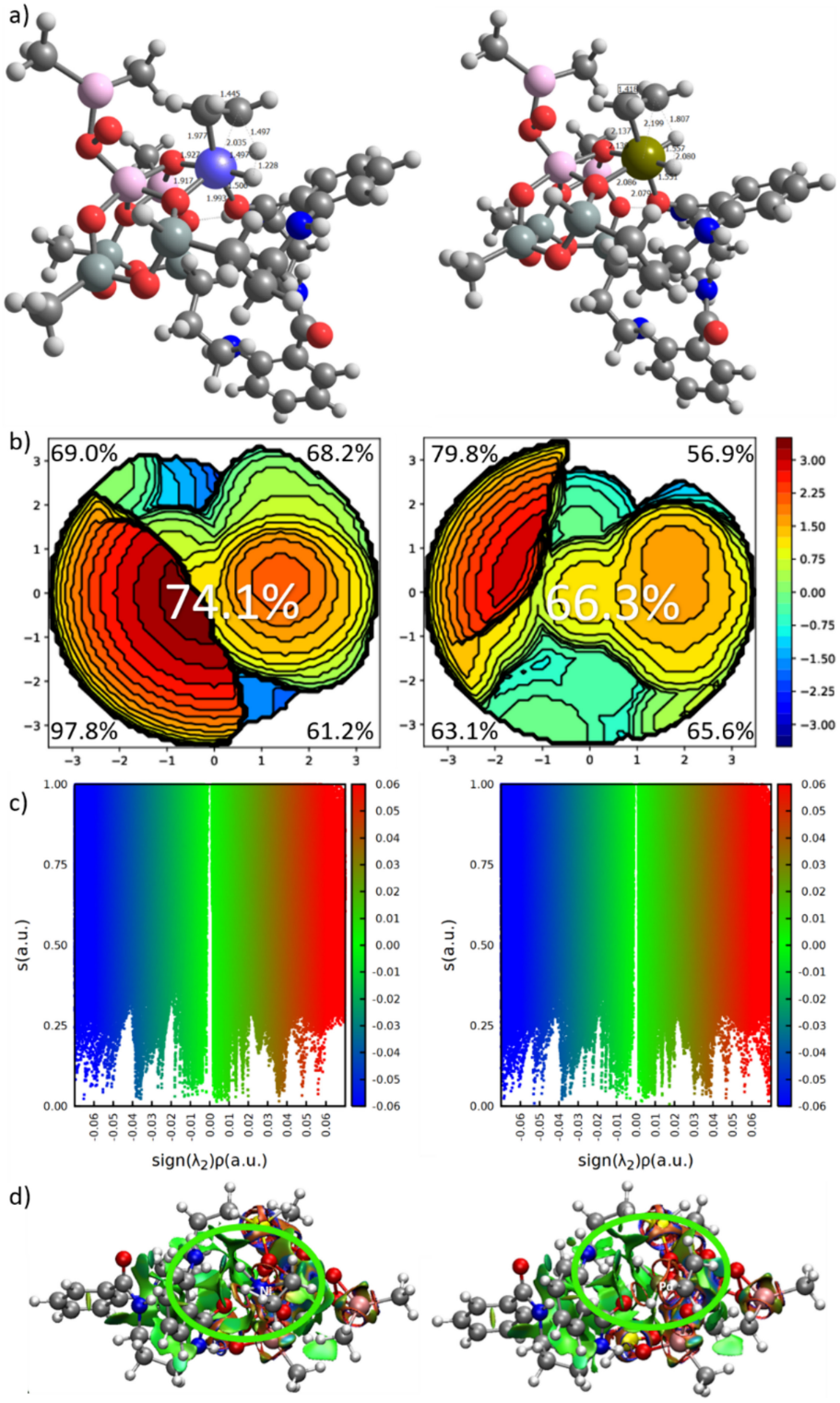

FIGURE 9 | For the computed TS **III–IV** for Ni (left) and Pd (right). (a) Optimized structures at the BP86-D3/Def2SVP-SDD level of theory with selected distances in Å. (b) Steric maps of the xy plane, featuring the H that is transferred at the center, with a radius of 3.5 Å, the metal atom providing it at the xz axis, and the C atoms where the H atom is transferred in the xz plane; curves are indicated in Å; and NCI plots (see Figure S1 for the NCI plots of the rdi **II**). (c) 2D and (d) 3D plots of the reduced density gradient (s) versus sign $(\lambda_2)\rho$, in a.u.

Kinetically, the energy difference between the two metals is disproportionately large [62], and we must ensure this is not an artifact. Simply replacing Pd with Ni, thereby moving from the second to the first series of transition metals, should result in a smaller difference. Structurally, the rate-determining step (rds) appears to hinge on the TS **III**–**IV**. Here, we observe an unexpected structural transformation. For Pd, the metal center exhibits almost perfect octahedral symmetry, whereas for Ni, we surprisingly see a trigonal bipyramidal structure (see Figure 9a). In this structure, the base includes two oxygen atoms and the previously olefinic ligand, whereas the two apical positions are occupied by the remaining oxygen atom and in trans a molecular hydrogen moiety. This distortion is so pronounced that the H···H distance, which is 2.080 Å for Pd, drops to 1.228 Å for Ni. Consequently, several other distances and angles differ significantly, making Ni kinetically disadvantaged. Cavallo et al.'s steric maps [63] further confirm the challenging situation for Ni, showing a $\%V_{Bur}$ index of 74.1% at the hydrogen transfer position, compared to just 66.3% for Pd (see Figure 9b) [64]. The quadrant analysis reveals one particularly hindered quadrant for Ni at 97.8%, underscoring the complete redistribution of ligands that hinders H transfer. For comparison, this highly hindered quadrant is only 63.1% for Pd, although another quadrant reaches 79.8%, whereas for Ni, it is only 69%. This indicates a total distortion of the metal center based on the steric map orientation.

Shifting the focus to natural population analysis (NPA) charges, for Ni, we see charges of 1.007, 0.794, and 0.610 e for intermediates **I**–**III** and 0.294 e at TS **III**–**IV**, finishing at 0.563 and 0.958 e for **IV** and **V** and 0.634 e for TS **IV**–**V**. For Pd, the situation is entirely different, with charges of 0.867, 0.661, 0.526, 0.567, and 0.726 e for **I**–**V** and 0.310 and 0.611 e for the two transition states, respectively. The key difference is that for Ni, the reaction involves a much greater charge redistribution, with a range of 0.713 e, compared to only 0.557 e for Pd.

Finally, a non-covalent interaction (NCI) analysis, depicted in Figure 9c for the 3D NCI plots of TS **III**–**IV** [65, 66], reveals a slightly higher number of non-covalent interactions in the case of Ni. This is further illustrated in the 2D NCI plots in Figure 9d, where there is a notably greater presence of favorable interactions in the range of 0.00 to −0.02 a.u. for Pd.

4 | Conclusions

To motivate the need for a catalytic system in the hydrotreating of PAO with higher efficiency, a family of extruded heterogeneous Pd catalysts were synthesized and fully characterized. In summary, we have successfully attained the regio-controlled hydrogenation of PAO using Pd catalyst on the extruded γ-Al_2O_3. For this purpose, we prepared extruded γ-Al_2O_3 with moderate surface areas and porosities. It is also necessary to point out that these alumina extrudates were found as a suitable support for the preparation of catalysts without changes in the surface chemical properties. According to the result, palladium/γ-Al_2O_3 catalyst was active in PAO hydrofinishing, compared to Ni/γ-Al_2O_3 catalyst under identical condition. It should be noted that we achieved a high degree of hydrofinishing (90%) in the presence of this catalyst by optimizing the hydrogenation conditions including catalyst loading = 5 wt. %, p = 12 bar, T = 130°C, and t = 7 h.

DFT analysis was conducted to understand why the Ni system performs worse in hydrogenation reactions. The Pd system showed a significantly lower energy barrier for hydrogen migration compared to Ni, indicating a kinetic preference for Pd. Structural analysis highlighted that the Pd center maintains an almost perfect octahedral symmetry, whereas Ni adopts a distorted trigonal bipyramidal structure, resulting in kinetic disadvantages for Ni. Steric and NPA further confirmed these findings, showing greater charge redistribution and steric hindrance for Ni.

Acknowledgments

The authors appreciate support of Iran Polymer and Petrochemical Institute. A.P. is a Serra Húnter Fellow, and ICREA Academia Prize 2019, and thanks the Spanish MINECO for project PID2021-127423NB-I00 and the Generalitat de Catalunya for project 2021SGR623. Computational time at the MARENOSTRUM supercomputer (QHS-2022-3-0029) has been provided by the Barcelona Supercomputing Centre through a grant from Red Española de Supercomputación.

Data Availability Statement

The data that support the findings of this study are available from the corresponding author upon reasonable request.

References

1. R. González, J. L. Viesca, A. Hernández Battez, M. Hadfield, A. Fernández-González, and M. Bartolomé, "Two Phosphonium Cation-Based Ionic Liquids as Lubricant Additive to a Polyalphaolefin Base Oil," *Journal of Molecular Liquids* 293 (2019): 111536.

2. J. M. Hogg, A. Ferrer-Ugalde, F. Coleman, and M. Swadźba-Kwaśny, "Borenium Ionic Liquids as Alternative to BF_3 in Polyalphaolefins (PAOs) Synthesis," *ACS Sustainable Chemistry & Engineering* 7 (2019): 15044–15052.

3. S. Ray, P. V. Rao, and N. V. Choudary, "Poly-α-Olefin-Based Synthetic Lubricants: A Short Review on Various Synthetic Routes," *Lubrication Science* 24 (2012): 23–44.

4. N. Nunn, Z. Mahbooba, M. G. Ivanov, D. M. Ivanov, D. W. Brenner, and O. Shenderova, "Tribological Properties of Polyalphaolefin Oil Modified With Nanocarbon Additives," *Diamond and Related Materials* 54 (2015): 97–102.

5. S. S. A. Kheljania, K. Didehbana, M. Ataib, et al., "In-Situ Photo-Crosslinkable Elastomer Based on Polyalphaolefin/Halloysite Nanohybrid," *Journal of Colloid and Interface Science* 659 (2024): 751–766.

6. M. Alleshagh, S. Sadjadi, H. Arabi, N. Bahri-Laleh, and E. Monflier, "Pd on Ligand-Decorated Chitosan as an Efficient Catalyst for Hydrofinishing polyalphaolefins: Experimental and Computational Studies," *Journal of Physics and Chemistry of Solids* 164 (2022): 110611.

7. M. Tabrizi, S. Sadjadi, G. Pareras, M. Nekoomanesh-Haghighi, N. Bahri-Laleh, and A. Poater, "Efficient Hydro-Finishing of Polyalfaolefin Based Lubricants Under Mild Reaction Condition Using Pd on Ligands Decorated Halloysite," *Journal of Colloid and Interface Science* 581 (2021): 939–953.

8. A. Hanifpour, N. Bahri-Laleh, A. Mohebbi, and M. Nekoomanesh-Haghighi, "Oligomerization of Higher α-Olefins to Poly(α-Olefins)," *Iranian Polymer Journal* 31 (2022): 107–126.

9. E. V. Parkhomchuk, A. I. Lysikov, A. G. Okunev, et al., "Meso/Macroporous CoMo Alumina Pellets for Hydrotreating of Heavy Oil," *Industrial and Engineering Chemistry Research* 52 (2013): 17117–17125.

10. S. Karimi, N. Bahri-Laleh, G. Pareras, S. Sadjadi, M. Nekoomanesh-Haghighi, and A. Poater, "Pd on Nitrogen Rich Polymer–Halloysite Nanocomposite as an Environmentally Benign and Sustainable Catalyst for Hydrogenation of Polyalfaolefin Based Lubricants," *Journal of Industrial and Engineering Chemistry* 97 (2021): 441–451.

11. A. Bayat, S. Sadjadi, H. Arabi, and N. Bahri-Laleh, "Dual-Task Composite of Halloysite and Ionic Liquid for the Synthesis and Hydrogenation of Polyalphaolefins," *Research on Chemical Intermediates* 48 (2022): 3171–3188.

12. A. Shams, S. Sadjadi, J. Duran, S. Simon, A. Poater, and N. Bahri-Laleh, "Effect of Support Hydrophobicity of Halloysite-Based Catalysts on the Polyalphaolefin Hydrofinishing Performance," *Applied Organometallic Chemistry* 36 (2022): e6719.

13. S. Sadjadi, F. Koohestani, and N. Bahri-Laleh, "Pd Immobilization on the Multi-amine Functionalized Halloysite as an Efficient Catalyst for Hydrogenation Reaction: An Experimental and Computational Study," *Applied Clay Science* 192 (2020): 105645.

14. K. Toshtay, A. Auyezov, Y. Aubakirov, et al., "Palladium–Nickel Supported and Palladated Activated Diatomite as an Efficient Catalyst for Poly-α-olefins Hydrogenation," *Catalysis Surveys from Asia* 27 (2023): 296–305.

15. N. M. Stuart and K. Sohlberg, "The Microstructure of γ-Alumina," *Energies* 14 (2021): 6472.

16. D. Trimm and A. Stanislaus, "The Control of Pore Size in Alumina Catalyst Supports: A Review," *Applied Catalysis* 21 (1986): 215–238.

17. M. Trueba and S. P. Trasatti, "γ-Alumina as a Support for Catalysts: A Review of Fundamental Aspects," *European Journal of Inorganic Chemistry* 2005 (2005): 3393–3403.

18. E. G. S. Junior, V. Haber Perez, I. Reyero, A. Serrano-Lotina, and O. Rodriguez Justo, "Biodiesel Production From Heterogeneous Catalysts Based K2CO3 Supported on Extruded γ-Al2O3," *Fuel* 241 (2019): 311–318.

19. G. Grzybek, S. Wójcik, K. Ciura, et al., "Influence of Preparation Method on Dispersion of Cobalt Spinel Over Alumina Extrudates and the Catalyst deN 2 O Activity," *Applied Catalysis B: Environmental* 210 (2017): 34–44.

20. M. Karimi, H. Arabi, and S. Sadjadi, "New Advances in Olefin Homo and Copolymerization Using Neutral, Single Component Palladium/Nickel Complexes Ligated by a Phosphine-Sulfonate," *Journal of Catalysis* 412 (2022): 59–70.

21. V. Singh, S. Takami, K. Minami, D. Hojo, and T. Adschiri, "Hybridisation of Sebacic Acid on the Surface of γ-Alumina Nanoparticles in Sub- and Supercritical Water," *Zeitschrift fur Naturforschung B* 65 (2010): 1045–1050.

22. H. Mills and S. Blackburn, "Rheological Behaviour of γ-Alumina/Boehmite Pastes," *Chemical Engineering Research and Design* 80 (2002): 464–470.

23. Z. Asadi, S. Sadjadi, N. Bahri-Laleh, and M. Nekoomanesh-Haghighi, "The Mono and Bimetallic Catalysts for Hydrogenation of PAO Lubricants," *ChemistrySelect* 8 (2023): e202301678.

24. A. Bayat, S. Sadjadi, H. Arabi, and N. Bahri-Laleh, "Catalytic Hydrofinishing of Polyalphaolefins Under Mild Condition Using Pd on Amino Acid-Functionalized Clay: Study of the Kinetic Parameters," *Inorganic Chemistry Communications* 144 (2022): 109923.

25. S. Escayola, N. Bahri-Laleh, and A. Poater, "%VBurindex and Steric Maps: From Predictive Catalysis to Machine Learning," *Chemical Society Reviews* 53 (2024): 853–882.

26. R. Monreal-Corona, A. Pla-Quintana, and A. Poater, "Predictive Catalysis: A Valuable Step Towards Machine Learning," *Trends in Chemistry* 5 (2023): 935–946.

27. M. Zarezadeh-Mehrizi, A. Afshar Ebrahimi, and A. Rahimi, "Preparation of Extruded Alumina With Suitable Crushing Strength and Good Stability," *Scientia Iranica* 25 (2018): 1434–1439.

28. N. van Garderen, F. J. Clemens, C. G. Aneziris, and T. Graule, "Improved γ-Alumina Support Based Pseudo-Boehmite Shaped by Micro-Extrusion Process for Oxygen Carrier Support Application," *Ceramics International* 38 (2012): 5481–5492.

29. F. Azzolina-Jury, "Novel Boehmite Transformation Into γ-Alumina and Preparation of Efficient Nickel Base Alumina Porous Extrudates for Plasma-Assisted CO2 Methanation," *Journal of Industrial and Engineering Chemistry* 71 (2019): 410–424.

30. Z. Asadi, S. Sadjadi, M. Nekoomanesh-Haghighi, et al., "Lubricant Hydrogenation Over a Functionalized Clay-Based pd Catalyst: A Combined Computational and Experimental Study," *Applied Organometallic Chemistry* 36 (2022): e6850.

31. M. Alleshagh, S. Sadjadi, H. Arabi, N. Bahri-Laleh, and E. Monflier, "Palladated Chitosan-Halloysite Bead as an Efficient Catalyst for Hydrogenation of Lubricants," *Materials Chemistry and Physics* 278 (2022): 125506.

32. S. Karimi, S. Sadjadi, N. Bahri-Laleh, and M. Kekoomanesh-Haghighi, "New Less-Toxic Halloysite-Supported Ionic Liquid/$AlCl_3$ Oligomerization Catalysts: A Comparative Study on the Effects of Various Ionic Liquids on the Properties of Polyalphaolefins," *Molecular Catalysis* 509 (2021): 111648.

33. M. Tabrizi, N. Bahri-Laleh, S. Sadjadi, and M. Nekoomanesh-Haghighi, "The Effect of Ionic Liquid Containing $AlCl_3$ Catalytic Systems on the Microstructure and Properties of Polyalphaolefin Based Lubricants," *Journal of Molecular Liquids* 335 (2021): 116299.

34. M. Mashayekhi, S. Talebi, S. Sadjadi, and N. Bahri-Laleh, "Production of Polyalfaolefin-Based Lubricants Using New (Poly)ionic Liquid /$AlCl_3$ Catalysts as Environmentally Friendly Alternatives to Commercial $AlCl_3$ Route," *Applied Catalysis A: General* 623 (2021): 118274.

35. M. J. Frisch, G. W. Trucks, H. B. Schlegel, et al., *Gaussian 16, Revision C.01* (Wallingford CT: Gaussian, Inc., 2016).

36. A. D. Becke, "Density-Functional Exchange-Energy Approximation With Correct Asymptotic Behavior," *Physical Review A* 38 (1988): 3098–3100.

37. J. P. Perdew, "Density-Functional Approximation for the Correlation Energy of the Inhomogeneous Electron Gas," *Physical Review B* 33 (1986): 8822–8824.

38. S. Grimme, J. Antony, S. Ehrlich, and H. Krieg, "A Consistent and Accurateab Initioparametrization of Density Functional Dispersion Correction (DFT-D) for the 94 Elements H-Pu," *Journal of Chemical Physics* 132 (2010): 154104.

39. F. Weigend and R. Ahlrichs, "Balanced Basis Sets of Split Valence, Triple Zeta Valence and Quadruple Zeta Valence Quality for H to Rn: Design and Assessment of Accuracy," *Physical Chemistry Chemical Physics* 7 (2005): 3297–3305.

40. F. Weigend, "Accurate Coulomb-Fitting Basis Sets for H to Rn," *Physical Chemistry Chemical Physics* 8 (2006): 1057–1065.

41. U. Häussermann, M. Dolg, H. Stoll, H. Preuss, P. Schwerdtfeger, and R. Pitzer, "Accuracy of Energy-Adjusted Quasirelativistic Ab Initio Pseudopotentials," *Molecular Physics* 78 (1993): 1211–1224.

42. W. Küchle, M. Dolg, H. Stoll, and H. Preuss, "Energy-Adjusted Pseudopotentials for the Actinides. Parameter Sets and Test Calculations for Thorium and Thorium Monoxide," *Journal of Chemical Physics* 100 (1994): 7535–7542.

43. T. Leininger, A. Nicklass, H. Stoll, M. Dolg, and P. Schwerdtfeger, "The Accuracy of the Pseudopotential Approximation. II. A Comparison of Various Core Sizes for Indium Pseudopotentials in Calculations for Spectroscopic Constants of InH, InF, and InCl," *Journal of Chemical Physics* 105 (1996): 1052–1059.

44. R. L. Martin, P. J. Hay, and L. R. Pratt, "Hydrolysis of Ferric Ion in Water and Conformational Equilibrium," *Journal of Physical Chemistry A* 102 (1998): 3565–3573.

45. A. Poater, E. Pump, S. V. C. Vummaleti, and L. Cavallo, "The Right Computational Recipe for Olefin Metathesis With Ru-Based Catalysts: The Whole Mechanism of Ring-Closing Olefin Metathesis," *Journal of Chemical Theory and Computation* 10 (2014): 4442–4448.

46. S. Manzini, A. Poater, D. J. Nelson, L. Cavallo, A. M. Z. Slawin, and S. P. Nolan, "Insights Into the Decomposition of Olefin Metathesis Precatalysts," *Angewandte Chemie, International Edition* 53 (2014): 8995–8999.

47. Y. Minenkov, E. Chermak, and L. Cavallo, "Troubles in the Systematic Prediction of Transition Metal Thermochemistry With Contemporary Out-of-the-Box Methods," *Journal of Chemical Theory and Computation* 12 (2016): 1542–1560.

48. A. D. Becke, "Density-Functional Thermochemistry. III. The Role of Exact Exchange," *Journal of Chemical Physics* 98 (1993): 5648–5652.

49. C. Lee, W. Yang, and R. G. Parr, "Development of the Colle-Salvetti Correlation-Energy Formula Into a Functional of the Electron Density," *Physical Review B* 37 (1988): 785–789.

50. P. J. Stephens, F. J. Devlin, C. F. Chabalowski, and M. J. Frisch, "Ab Initio Calculation of Vibrational Absorption and Circular Dichroism Spectra Using Density Functional Force Fields," *Journal of Physical Chemistry* 98 (1994): 11623–11627.

51. T. H. Dunning, Jr., "Gaussian Basis Sets for Use in Correlated Molecular Calculations. I. The Atoms Boron Through Neon and Hydrogen," *Journal of Chemical Physics* 90 (1989): 1007–1023.

52. K. Atrak, A. Ramazani, and S. Taghavi Fardood, "Green Synthesis of Amorphous and Gamma Aluminum Oxide Nanoparticles by Tragacanth Gel and Comparison of Their Photocatalytic Activity for the Degradation of Organic Dyes," *Journal of Materials Science: Materials in Electronics* 29 (2018): 8347–8353.

53. S. Kiani, M. Mansouri Zadh, S. Khodabakhshi, A. Rashidi, and J. Moghadasi, "Newly Prepared Nano Gamma Alumina and Its Application in Enhanced Oil Recovery: An Approach to Low-Salinity Waterflooding," *Energy and Fuels* 30 (2016): 3791–3797.

54. S. Beshkoofeh, "The Preparation of FeMo/γ-Al_2O_3 Extruded Catalyst and Optimization of the Operating Conditions of the ODS of Light Oil Naphtha," *Physical Chemistry Research* 11 (2023): 191–202.

55. S. Shahidian, K. Zare, and S. M. Mousavi Safavi, "Modification of Mesopore Extrudate Gamma Alumina Through Thermal Ammonia Treatment," *Iranian journal of chemistry and chemical engineering* 39 (2020): 61–69.

56. E. P. Fernandes, T. S. Silva, C. M. Carvalho, et al., "Efficient Adsorption of Dyes by γ-Alumina Synthesized From Aluminum Wastes: Kinetics, Isotherms, Thermodynamics and Toxicity Assessment," *Chemical Engineer* 9 (2021): 106198.

57. M. Salimi, A. Tavasoli, and L. Rosendahl, "Optimization of γ-Alumina Porosity via Response Surface Methodology: The Influence of Engineering Support on the Performance of a Residual Oil Hydrotreating Catalyst," *Microporous and Mesoporous Materials* 299 (2020): 110124.

58. A. Faraji Alamouti, M. Nadafan, Z. Dehghani, M. H. Majles Ara, and A. Veijdani Noghreiyan, "Structural and Optical Coefficients Investigation of γ-Al_2O_3 Nanoparticles Using Kramers-Kronig Relations and Z–Scan Technique," *Journal of Asian Ceramic Societies* 9 (2021): 366–373.

59. Y. Zhang, Y. Zhang, and Z. Jian, "A Comprehensive Picture on Chain Walking Olefin Polymerization," *Polymer* 265 (2023): 125578.

60. C. Alberoni, M. C. D'Alterio, G. Balducci, et al., "Tunable "In-Chain" and "at the end of the Branches" Methyl Acrylate Incorporation in the Polyolefin Skeleton Through pd(II) catalysis," *ACS Catalysis* 12 (2022): 3430–3443.

61. A. Rahbar, B. Falcone, G. Pareras, M. Nekoomanesh-Haghighi, N. Bahri-Laleh, and A. Poater, "Chain Walking in the $AlCl_3$ Catalyzed Cationic Polymerization of α-Olefins," *ChemPlusChem* 88 (2023): e202200432.

62. G. M. Meconi, S. V. C. Vummaleti, J. A. Luque-Urrutia, et al., "Mechanism of the Suzuki–Miyaura Cross-Coupling Reaction Mediated by [Pd(NHC)(allyl)Cl] Precatalysts," *Organometallics* 36 (2017): 2088–2095.

63. Z. Falivene, A. Cao, L. Petta, et al., "Towards the Online Computer-Aided Design of Catalytic Pockets," *Nature Chemistry* 11 (2019): 872–879.

64. J. Bosson, A. Poater, L. Cavallo, and S. P. Nolan, "Mechanism of Racemization of Chiral Alcohols Mediated by 16-Electron Ruthenium Complexes," *Journal of the American Chemical Society* 132 (2010): 13146–13149.

65. E. R. Johnson, S. Keinan, P. Mori-Sanchez, J. Contreras-Garcia, A. J. Cohen, and W. T. Yang, "Revealing Noncovalent Interactions," *Journal of the American Chemical Society* 132 (2010): 6498–6506.

66. J. Contreras-Garcia, E. R. Johnson, S. Keinan, et al., "NCIPLOT: A Program for Plotting Noncovalent Interaction Regions," *Journal of Chemical Theory and Computation* 7 (2011): 625–632.

Supporting Information

Additional supporting information can be found online in the Supporting Information section.